

Interplay of activity and non-reciprocity in tracer dynamics: From non-equilibrium fluctuation-dissipation to giant diffusion

Subhajit Paul^{1,*} and Debasish Chaudhuri^{2,3,†}

¹*Department of Physics and Astrophysics, University of Delhi, Delhi 110007, India*

²*Institute of Physics, Sachivalaya Marg, Bhubaneswar-751005, India*

³*Homi Bhabha National Institute, Anushaktinagar, Mumbai-400094, India*

(Dated: January 8, 2026)

Non-reciprocal interactions play a key role in shaping transport in active and passive systems, giving rise to striking nonequilibrium behavior. Here, we study the dynamics of a tracer – active or passive – embedded in a bath of active or passive particles, coupled through non-reciprocal interactions. Starting from the microscopic stochastic dynamics of the full system, we derive an overdamped generalized Langevin equation for the tracer, incorporating a non-Markovian memory kernel that captures bath-mediated correlations. This framework enables us to compute the tracer's velocity and displacement response, derive a generalized nonequilibrium fluctuation-dissipation relation that quantifies deviations from equilibrium behavior, and determine the mean-squared displacement (MSD). We find that while the MSD becomes asymptotically diffusive, the effective diffusivity depends non-monotonically on the degree of non-reciprocity and diverges at an intermediate value. This regime of giant diffusivity provides a generic mechanism for enhanced transport in active soft matter and has direct implications for biological systems exhibiting chase-and-run or predator-prey interactions. Our analytical predictions are supported by numerical simulations of active Brownian particles, highlighting experimentally accessible signatures of non-reciprocal interactions in soft matter.

I. INTRODUCTION

Tracer particles have long been used as effective probes to explore the microscopic and mesoscopic properties of complex media. By tracking the trajectories of these tracers and analyzing key observables like the mean-squared displacement (MSD), one can identify different transport regimes, such as ballistic, diffusive, subdiffusive, and superdiffusive motion. This analysis also helps uncover dynamical transitions that reveal underlying relaxation mechanisms occurring at various time scales [1–15]. This methodology forms the foundation of both passive and active microrheology [1, 2], and has been widely applied to diverse experimental systems, from colloidal suspensions and crowded environments to biological systems and living matter [3, 4, 6, 7, 16–18].

In equilibrium systems, the motion of tracer particles is typically governed by Brownian motion, where diffusivity, mobility, and temperature are all connected through the fluctuation-dissipation relation (FDR) [19]. However, when systems move away from equilibrium, this familiar picture changes dramatically. In active and driven systems, continuous energy input at the microscopic level disrupts detailed balance, leading to anomalous transport behaviors, non-Gaussian fluctuations, and violations of the equilibrium FDR. This type of behavior has been widely studied in systems where tracers are immersed in active baths, such as those composed of bacteria, active colloids, or active Brownian particles. These studies have revealed intriguing phenomena like enhanced diffusion, Lévy-like statistics, and dynamic crossovers driven by the system's activity and persistence [3–5, 20–22].

Tracer-based methods have proven especially powerful in biological systems, where the surrounding environment is both active and heterogeneous. Experiments and theoretical studies have uncovered anomalous diffusion in living cells [7, 23–26], non-equilibrium fluctuations driven by cytoskeletal activity [25, 26], and complex transport behaviors during cell migration [9, 27]. These findings have motivated extensive theoretical work aimed at understanding key concepts like effective temperatures, modified Einstein relations, and generalized response functions in active systems [28–35]. In addition, there has been a focus on how activity influences viscous drag, mobility, and kinetic temperature [36–40]. Despite these advances, however, a unified framework that connects microscopic interactions to tracer transport remains elusive.

Most theoretical models of tracer-bath dynamics are built on the assumption of reciprocal interactions between the tracer and the bath, whether explicitly or implicitly. In standard system-bath models, reciprocal bilinear couplings are assumed, which enforce an action-reaction symmetry [41, 42]. Even when these models are extended to active baths,

* spaul@physics.du.ac.in

† debc@iopb.res.in

non-equilibrium effects are typically introduced through mechanisms like self-propulsion, colored noise, or modified dissipation, while the interaction forces themselves still assume reciprocity [5, 21, 43]. This assumption limits the resulting dynamics and may not fully capture the behavior of many active or biological systems.

Recent advances in active matter have highlighted that non-reciprocal interactions – which break the action-reaction symmetry – are a common feature in driven systems, not just a rare exception [44, 45]. These interactions naturally emerge from hydrodynamic couplings, diffusive chemical fields, elastic deformations, and information-mediated responses, giving rise to new and often unexpected behaviors [46–52]. Non-reciprocal interactions have been both theoretically and experimentally observed in systems like chemically active and catalytic colloids [53–58], vision-based or programmable interactions [49, 59–62], and quorum-sensing active particles [63, 64]. In biological and ecological contexts, such interactions are key to behaviors like chase-and-run dynamics, predator-prey interactions, and pursuit-evasion strategies [65–71].

While there has been growing interest in how non-reciprocal interactions influence collective behaviors – like pattern formation, traveling states, and non-reciprocal phase transitions [46–48] – their effects on single-particle transport, especially tracer dynamics, remain relatively less explored. This is an important gap, as tracer motion offers a direct and experimentally accessible way to study non-equilibrium environments. Understanding how non-reciprocal interactions affect response, fluctuations, and transport properties is crucial for accurately interpreting microrheological measurements in active and biological systems.

In this work, we address this problem by introducing a generalized system-bath framework for tracer dynamics that incorporates explicitly non-reciprocal interactions. We consider a tracer particle that may itself be passive or active and couple it to a bath whose constituents can be continuously tuned between passive and active limits via a persistence parameter. This approach allows us to interpolate seamlessly between equilibrium-like and strongly non-equilibrium baths, while isolating the specific effects of non-reciprocity in the interactions themselves.

Using this framework, we derive the overdamped generalized Langevin equation of motion [41, 42] for the tracer, and we obtain analytical expressions for its linear response function. This leads to a generalized non-equilibrium fluctuation-dissipation relation, as well as an expression for the mean-squared displacement. Our results clearly show how the equilibrium fluctuation-dissipation relation is violated and highlight how non-reciprocal couplings change the way response and fluctuations are related. Specifically, we find that the tracer’s long-time diffusion constant depends non-monotonically on the strength of non-reciprocity, even when other bath parameters are held constant.

For a certain range of non-reciprocal couplings, which correspond to chase-and-run dynamics, we predict that the tracer diffusivity will diverge, signaling the onset of giant diffusion driven entirely by non-reciprocal interactions. We confirm these predictions with numerical simulations of a simple microscopic model involving active Brownian particles, and find strong agreement across different parameter regimes. Our results establish non-reciprocity as a key factor in controlling tracer transport, extending traditional system-bath models [41, 42] to a wider range of active, biological, and information-driven systems.

II. MODEL FOR TRACER COUPLED TO BATH PARTICLES

We consider a tracer s at position X_s coupled to a $i = 1, 2, \dots, N$ particle bath with positions denoted by $\{x_i\}$. Their joint evolution can be expressed as

$$\begin{aligned} \frac{dx_i}{dt} &= -\lambda(x_i - X_s) + \xi_i \\ \frac{dX_s}{dt} &= -\Lambda \sum_{i=1}^N (X_s - x_i) + \zeta \end{aligned} \quad (1)$$

where two independent coupling constants λ and Λ can model generic non-conservative interaction. In the limit of $\lambda = \Lambda$, the interaction is reciprocal and any departure from this equality describes non-reciprocity. Before proceeding, we note that for $\lambda, \Lambda > 0$ the solution $x_i = X_s$ is a unique stable fixed point, as in the reciprocal case. This picture breaks down when the non-reciprocity parameter $\chi = \Lambda/\lambda$ becomes negative, rendering the solution unstable for one of the variables. As we show below, it is precisely in this regime that the most striking qualitative effect – giant diffusion – emerges.

For simplicity, we consider a non-interacting bath. The particles can be continuously tuned from passive to active by adjusting the statistical properties of the random noises $\xi_i(t)$ and $\zeta(t)$. The model allows for changing the nature of the tracer and bath particles to generate the following four possibilities, (i) a passive tracer in a passive bath, (ii) a passive tracer in an active bath, (iii) an active tracer in a passive bath, (iv) an active tracer in an active bath.

Modeling active and passive particles and their noise correlations

Three related active particle models have been in use to describe self propelled elements, these are active Brownian particles (ABP), run-and-tumble particles (RTP), and active Ornstein-Uhlenbeck particles (AOUP). All these models are equivalent up to the second moment. They can be described using a correlated random noise $\xi_i(t)$ representing the active velocity such that $\langle \xi_i(t) \rangle = 0$ and

$$\langle \xi_i(t) \xi_j(0) \rangle = A \exp(-t/\tau_a) \delta_{ij}, \quad (2)$$

where A denotes a strength of activity and τ_a is the persistence time.

Here we summarize the three models in one dimension [14]. For RTP, particles move with active velocity v_0 with their orientation switching between ± 1 with rate α . This results in $A = v_0^2$ and $\tau_a = 1/2\alpha$. For ABP, the active velocity in one dimension is $v_i = v_0 \cos \theta_i$ with the orientation evolving as $\dot{\theta}_i = \sqrt{2D^{\text{rot}}} \eta_i(t)$ where $\eta_i(t)$ denotes a univariate Gaussian random noise and D^{rot} represents the rotational diffusion constant. This leads to $\langle v_i(t) v_j(0) \rangle = v_0^2 \delta_{ij} e^{-D^{\text{rot}} t}$. Thus, the strength of correlation $A = v_0^2$ and the persistence time $\tau_a = 1/D^{\text{rot}}$. Finally, in the AOUP model the active velocity evolves as $\tau_v \dot{v}_i = -v_i + \sqrt{2D} \eta_i(t)$ leading to $\langle v_i(t) v_j(0) \rangle = \delta_{ij} (D/\tau_v) \exp(-t/\tau_v)$. Thus giving $A = D/\tau_v \equiv v_0^2$ with persistence time $\tau_a = \tau_v$. In this case $\dot{x}_i = v_i$ gives MSD $\langle \Delta x^2(t) \rangle = 2D[t + \tau_v(e^{-t/\tau_v} - 1)]$ leading to the asymptotic diffusion $\langle \Delta x^2(t) \rangle = 2Dt$. Thus, we can summarize the two-time noise correlation corresponding to the three active particle models as

$$\langle \xi_i(t) \xi_j(0) \rangle = \delta_{ij} v_0^2 e^{-t/\tau_a} \quad (3)$$

where $\tau_a = 1/2\alpha$ for RTP, $\tau_a = 1/D^{\text{rot}}$ for ABP and $\tau_a = \tau_v$ for AOUP. Moreover, these models lead to a late time diffusivity $\mathcal{D} = v_0^2 \tau_a$.

The same noise property can be used to model active tracer by replacing ξ_i with ζ , as mentioned in Eq. (3). Moreover, it is straightforward to obtain the equilibrium limit by taking $\tau_a \rightarrow 0$ and $v_0 \rightarrow \infty$ such that $\mathcal{D} = v_0^2 \tau_a$ is a constant equal to the equilibrium diffusivity $D = k_B T / \gamma$, with T corresponds to the temperature. One can then rewrite Eq. (3) as $\langle \xi_i(t) \xi_j(t') \rangle = \delta_{ij} 2D \frac{1}{2\tau_a} e^{-|t-t'|/\tau_a} = \delta_{ij} 2D \delta(t-t')$, in the limit of $\tau_a \rightarrow 0$.

In the following, we distinguish the tracer and bath particles by denoting their active speed and persistence time using the symbols (v_s, τ_s) and (v_b, τ_b) , respectively.

III. DYNAMICS OF THE TRACER

The tracer dynamics associated with Eq. (1) can be obtained using the formal solution of the bath particles

$$x_i(t) = x_i(0) e^{-\lambda t} + \int_0^t [\xi_i(t') + \lambda X_s(t')] e^{-\lambda(t-t')} dt' \quad (4)$$

in the dynamics of X_s in Eq.(1). After some simplifications, we obtain (see Appendix A):

$$\frac{dX_s}{dt} + N\Lambda \int_0^t \mathcal{G}(t-t') \frac{dX_s(t')}{dt'} dt' = \zeta + N\Lambda \int_0^t \mathcal{G}(t-t') \xi(t') dt', \quad (5)$$

where the Green's function $\mathcal{G}(t-t') = e^{-\lambda(t-t')}$. Note that the parameter λ appearing in the Green's function characterizes how the bath particles couple to the tracer. This equation involves only $X_s(t)$, integrating out the bath degrees of freedom. The terms on the right hand side describe the effective noise on the tracer.

The presence of $\mathcal{G}(t-t')$ in the second term makes the dynamics of X_s non-Markovian. Exploiting the finite temporal range of the memory kernel, characterized by the timescale λ^{-1} , we can rewrite Eq. (5) by extending the lower limits of the integrals to $t \rightarrow -\infty$, yielding

$$\frac{dX_s}{dt} + N\Lambda \int_{-\infty}^t \frac{dX_s(t')}{dt'} \mathcal{G}(t-t') dt' = \zeta(t) + N\Lambda \int_{-\infty}^t \xi(t') \mathcal{G}(t-t') dt' \equiv \eta_s^{\text{eff}}(t), \quad (6)$$

In a later section, we use this equation to calculate the MSD of the tracer.

The right hand side of this equation depends on the stochastic noise $\zeta(t)$ and $\xi(t)$. Thus, interpreting these terms as effective noise $\eta_s^{\text{eff}}(t) = \zeta(t) + \zeta_b(t)$ where $\zeta(t)$ is the intrinsic noise, active or passive, acting on the tracer, while

the contribution from the bath $\zeta_b(t) = N\Lambda \int_{-\infty}^t \xi(t')\mathcal{G}(t-t')dt'$. We proceed to obtain the mean and the two-time correlation for $\eta_s^{\text{eff}}(t)$. From the definition it follows that $\langle \eta_s^{\text{eff}}(t) \rangle = 0$. The two-time correlation is written as,

$$\langle \eta_s^{\text{eff}}(t_1) \eta_s^{\text{eff}}(t_2) \rangle = \langle \zeta(t_1) \zeta(t_2) \rangle + \langle \zeta_b(t_1) \zeta_b(t_2) \rangle, \quad (7)$$

for which the cross term $\langle \zeta(t_1) \zeta_b(t_2) \rangle = 0$.

A. Characterizing the noise

The two-time noise correlation for the tracer can be expressed as

$$\langle \zeta(t_1) \zeta(t_2) \rangle = v_s^2 e^{-|t_1-t_2|/\tau_s} = \frac{\mathcal{D}_s}{\tau_s} e^{-|t_1-t_2|/\tau_s}, \quad (8)$$

where v_s and τ_s are the active velocity and the persistence time for the tracer, respectively; $\mathcal{D}_s = v_s^2 \tau_s$ denotes the effective diffusivity. In the limit of vanishing persistence $\tau_s \rightarrow 0$, and $v_s \rightarrow \infty$ keeping the effective diffusivity constant $\mathcal{D}_s = D_s$ the tracer behaves as a passive one. In this limit, we get

$$\lim_{\tau_s \rightarrow 0} \langle \zeta(t_1) \zeta(t_2) \rangle = 2D_s \delta(t_1 - t_2).$$

The general form of $\langle \zeta_b(t_1) \zeta_b(t_2) \rangle$ gives

$$\begin{aligned} \langle \zeta_b(t_1) \zeta_b(t_2) \rangle &= N^2 \Lambda^2 \int_{-\infty}^{t_1} \int_{-\infty}^{t_2} \langle \xi(t'_1) \xi(t'_2) \rangle \mathcal{G}(t_1 - t'_1) \mathcal{G}(t_2 - t'_2) dt'_1 dt'_2 \\ &= N^2 \Lambda^2 v_b^2 e^{-\lambda(t_1+t_2)} \int_{-\infty}^{t_1} \int_{-\infty}^{t_2} e^{-|t'_1-t'_2|/\tau_b} e^{\lambda(t'_1+t'_2)} dt'_1 dt'_2 \\ &= N^2 \Lambda^2 v_b^2 \left[\frac{\tau_b e^{-\lambda|t_2-t_1|}}{\lambda(1-\lambda^2\tau_b^2)} + \tau_b^2 \frac{e^{-|t_2-t_1|/\tau_b}}{(\lambda^2\tau_b^2-1)} \right]. \end{aligned} \quad (9)$$

In deriving the second step, we used Eq. (3). A straightforward algebraic manipulation then yields the final result shown in Eq. (9). Here, λ^{-1} and τ_b set the two correlation times.

Equation (7) therefore yields the general form of the effective noise correlation

$$\langle \eta_s^{\text{eff}}(t_1) \eta_s^{\text{eff}}(t_2) \rangle = \frac{\mathcal{D}_s}{\tau_s} e^{-|t_1-t_2|/\tau_s} + N^2 \Lambda^2 v_b^2 \left[\frac{\tau_b e^{-\lambda|t_2-t_1|}}{\lambda[1-\lambda^2\tau_b^2]} + \tau_b^2 \frac{e^{-|t_2-t_1|/\tau_b}}{[\lambda^2\tau_b^2-1]} \right] \quad (10)$$

Using the noise correlation for the bath particles (Eq. (9)), it is straightforward to analyze two limiting cases: the large-persistence (high-activity) regime and the equilibrium limit of vanishing persistence. In the high-persistence limit (large τ_b),

$$\langle \zeta_b(t_1) \zeta_b(t_2) \rangle_{\text{active}} = \left(\frac{N\Lambda}{\lambda} \right)^2 v_b^2 e^{-|t_2-t_1|/\tau_b} = \left(\frac{N\Lambda}{\lambda} \right)^2 \frac{\mathcal{D}_b}{\tau_b} e^{-|t_2-t_1|/\tau_b}, \quad (11)$$

where the effective diffusivity $\mathcal{D}_b = v_b^2 \tau_b$. In the limit of vanishing persistence, $\tau_b \rightarrow 0$, with $v_b \rightarrow \infty$ while keeping $\mathcal{D}_b = D_b$ fixed, we recover the equilibrium behavior, where the memory in the noise correlation is governed solely by the interaction,

$$\langle \zeta_b(t_1) \zeta_b(t_2) \rangle_{\text{passive}} = \left(\frac{N\Lambda}{\lambda} \right)^2 2D_b \frac{\lambda}{2} e^{-\lambda|t_2-t_1|}. \quad (12)$$

Furthermore, in the limit of large λ , the noise becomes uncorrelated, as $\frac{\lambda}{2} e^{-\lambda|t_2-t_1|}$ can be replaced by $\delta(t_1 - t_2)$. Here, λ denotes the one-way coupling of the bath particles to the tracer.

The calculations above illustrate the four possible scenarios arising from whether the bath particles and the tracer are active or passive. Accordingly, the terms in Eq. (7) corresponding to the tracer and bath noises are summarized in Table I for these four combinations.

TABLE I. The table presents the two-time noise correlations, $\langle \zeta(t_1)\zeta(t_2) \rangle$ and $\langle \zeta_b(t_1)\zeta_b(t_2) \rangle$, for both the tracer and the bath particles, distinguishing between active and passive cases.

Nature of the tracer	Nature of bath particles	$\langle \zeta(t_1)\zeta(t_2) \rangle$	$\langle \zeta_b(t_1)\zeta_b(t_2) \rangle$
Active	Active	$\frac{D_s}{\tau_s} e^{- t_1-t_2 /\tau_s}$	$\left(\frac{N\Lambda}{\lambda}\right)^2 \frac{D_b}{\tau_b} e^{- t_2-t_1 /\tau_b}$
Active	Passive	$\frac{D_s}{\tau_s} e^{- t_1-t_2 /\tau_s}$	$\left(\frac{N\Lambda}{\lambda}\right)^2 2D_b \frac{\lambda}{2} e^{-\lambda t_2-t_1 }$
Passive	Active	$2D_s \delta(t_1 - t_2)$	$\left(\frac{N\Lambda}{\lambda}\right)^2 \frac{D_b}{\tau_b} e^{- t_2-t_1 /\tau_b}$
Passive	Passive	$2D_s \delta(t_1 - t_2)$	$\left(\frac{N\Lambda}{\lambda}\right)^2 2D_b \frac{\lambda}{2} e^{-\lambda t_2-t_1 }$

B. Linear response

Velocity Response: The response function quantifies the changes in the velocity of a particle due to an external force. In the presence of a force $f(t)$, the Fourier transform of Eq. (6) (with $dX_s/dt = v(t)$) yields

$$\tilde{v}(\omega) + N\Lambda \tilde{v}(\omega) \tilde{\mathcal{G}}(\omega) = \tilde{\zeta}(\omega) + \tilde{\zeta}_b(\omega) + \tilde{f}(\omega), \quad (13)$$

where $\tilde{f}(\omega)$ is the Fourier transform of $f(t)$ and $\tilde{v}(\omega) = \int_{-\infty}^{\infty} dt e^{-i\omega t} v(t)$ with the inverse Fourier transform $v(t) = \frac{1}{2\pi} \int_{-\infty}^{\infty} d\omega e^{i\omega t} \tilde{v}(\omega)$. The Green's function $\tilde{\mathcal{G}}(\omega)$ is given by,

$$\tilde{\mathcal{G}}(\omega) = \int_{-\infty}^{\infty} e^{-\lambda t} e^{-i\omega t} dt = \frac{1}{\lambda + i\omega}; \quad \text{provided } \mathcal{G}(t) = 0 \text{ for } t < 0. \quad (14)$$

This equation gives the dynamical response $R_v(\omega)$ as

$$R_v(\omega) = \frac{\langle \tilde{v}(\omega) \rangle}{\tilde{f}(\omega)} = \frac{1}{1 + N\Lambda \tilde{\mathcal{G}}(\omega)} = \frac{\lambda + i\omega}{\lambda + N\Lambda + i\omega}, \quad (15)$$

from which the mobility can be obtained in the limit $\omega \rightarrow 0$ as

$$\mu_{\text{eff}} = R_v(\omega = 0) = \lim_{\omega \rightarrow 0} \frac{\langle \tilde{v}(\omega) \rangle}{\tilde{f}(\omega)} = \frac{1}{1 + N\Lambda \tilde{\mathcal{G}}(0)} = \frac{1}{1 + N\Lambda/\lambda}$$

Displacement response: Using Eq. (6) and the Fourier transform $\tilde{X}_s(\omega) = \int_{-\infty}^{\infty} X_s(t) e^{-i\omega t} dt$, the position response $R_x(\omega)$ can be written as

$$R_x(\omega) = \frac{\langle \tilde{X}_s(\omega) \rangle}{\tilde{f}(\omega)} = \frac{1}{i\omega(1 + N\Lambda \tilde{\mathcal{G}}(\omega))} = \frac{\lambda + i\omega}{i\omega(\lambda + N\Lambda + i\omega)}. \quad (16)$$

C. Generalized fluctuation-dissipation relation

The correlation function $C_v(\tau) = \langle v(t)v(t+\tau) \rangle$ is time-translation invariant in the steady state. Its Fourier transform $\tilde{C}_v(\omega)$ is defined as $\tilde{C}_v(\omega) = \int_{-\infty}^{\infty} C_v(t) e^{-i\omega t} dt$, with the inverse transform $C_v(t) = \frac{1}{2\pi} \int_{-\infty}^{\infty} \tilde{C}_v(\omega) e^{i\omega t} d\omega$. Thus, the velocity correlation in Fourier space can be written as

$$\begin{aligned} \langle \tilde{v}(\omega) \tilde{v}(\omega') \rangle &= \int_{-\infty}^{\infty} dt \int_{-\infty}^{\infty} dt' \langle v(t)v(t') \rangle e^{-i\omega t} e^{-i\omega' t'} \\ &= \int_{-\infty}^{\infty} dt \int_{-\infty}^{\infty} d\tau e^{-i\omega t} e^{-i\omega'(t+\tau)} C_v(\tau) = 2\pi \delta(\omega + \omega') \tilde{C}_v(\omega). \end{aligned} \quad (17)$$

In the absence of an external force the velocity mode is given by $\tilde{v}(\omega) = R_v(\omega)\eta_s^{\text{eff}}(\omega)$ where the effective noise $\eta_s^{\text{eff}}(\omega) = [\tilde{\zeta}(\omega) + \tilde{\zeta}_b(\omega)]$ is the sum of the two noise contributions. Using this, the two-point correlation function in Fourier space,

$$\langle \tilde{v}(\omega)\tilde{v}(\omega') \rangle = R_v(\omega)R_v(\omega') \langle \eta_s^{\text{eff}}(\omega)\eta_s^{\text{eff}}(\omega') \rangle \equiv 2\pi\delta(\omega + \omega') \tilde{C}_v(\omega), \quad (18)$$

where in the last step we used Eq. (17). Using the expressions for the noise correlations $\langle \tilde{\zeta}_b(\omega)\tilde{\zeta}_b(\omega') \rangle$ and $\langle \tilde{\zeta}(\omega)\tilde{\zeta}(\omega') \rangle$ from Eqs. (C5) and (C7) in Appendix-C, one finds the power spectral density

$$\tilde{C}_v(\omega) = \frac{1}{2\pi} \langle |\tilde{v}(\omega)|^2 \rangle = \mathcal{B}(\omega) |R_v(\omega)|^2 = \mathcal{B}(\omega) \frac{\lambda^2 + \omega^2}{(\lambda + N\Lambda)^2 + \omega^2} = \mathcal{B}(\omega) \frac{\lambda^2 + \omega^2}{N\Lambda\omega} \text{Im}[R_v(\omega)]. \quad (19)$$

where $\mathcal{B}(\omega)$ denotes the squared strength of the total noise $\eta_s^{\text{eff}}(\omega)$ and we used Eq. (15) in the last step. We now obtain $\mathcal{B}(\omega)$ by combining $\mathcal{B}_1(\omega)$ and $\mathcal{B}_2(\omega)$ from Eqs.(C6) and (C8) as

$$\mathcal{B}(\omega) = \frac{1}{2\pi} (\mathcal{B}_1(\omega) + \mathcal{B}_2(\omega)) = \left(\frac{N^2\Lambda^2}{\lambda^2 + \omega^2} \frac{2\mathcal{D}_b}{1 + \omega^2\tau_b^2} + \frac{2\mathcal{D}_s}{1 + \omega^2\tau_s^2} \right). \quad (20)$$

The result in Eq. (19) shows that the steady-state fluctuations $\tilde{C}_v(\omega)$ are governed by the dissipative (imaginary) part of the linear response $\text{Im}[R_v(\omega)]$, thereby establishing a generalized fluctuation-dissipation relation around the non-equilibrium steady state.

Before proceeding, we note that the effective diffusivity D_{eff} can be directly extracted from the generalized fluctuation-dissipation relation, using $\tilde{C}_v(\omega = 0) = 2D_{\text{eff}}$. This gives

$$D_{\text{eff}} = \frac{1}{(1 + N\Lambda/\lambda)^2} \left(\mathcal{D}_s + \mathcal{D}_b \frac{N^2\Lambda^2}{\lambda^2} \right) \quad (21)$$

which is consistent with the result obtained later from an explicit calculation of the mean-squared displacement.

In a similar manner, the generalized fluctuation-dissipation relation for the displacement response $R_x(\omega)$ and the corresponding power-spectral density $\tilde{C}_x(\omega)$ can be obtained,

$$\tilde{C}_x(\omega) = \frac{1}{2\pi} \langle |\tilde{X}_s(\omega)|^2 \rangle = \mathcal{B}(\omega) |R_x(\omega)|^2 = \mathcal{B}(\omega) \frac{\lambda^2 + \omega^2}{\omega[\omega^2 + \lambda(\lambda + N\Lambda)]} \text{Im}[R_x(\omega)]. \quad (22)$$

D. Departure from equilibrium

The the departure from equilibrium can be expressed as

$$\mathcal{I}_v(\omega) = \tilde{C}_v(\omega) - \tilde{C}_v^{\text{eq}}(\omega) \quad (23)$$

where

$$\tilde{C}_v^{\text{eq}}(\omega) = \mathcal{B}^{\text{eq}}(\omega) \frac{\lambda^2 + \omega^2}{N\lambda\omega} \text{Im}[R_v^{\text{eq}}(\omega)] = 2D_{\text{eq}} \left[1 + \frac{N^2\lambda^2}{\lambda^2 + \omega^2} \right] \frac{\lambda^2 + \omega^2}{(N+1)^2\lambda^2 + \omega^2} = 2D_{\text{eq}} \frac{\lambda^2(1+N^2) + \omega^2}{\lambda^2(1+N)^2 + \omega^2} \quad (24)$$

In the last step we used $\mathcal{B}^{\text{eq}}(\omega) = 2D_{\text{eq}} \left[1 + \frac{N^2\lambda^2}{\lambda^2 + \omega^2} \right]$ [72] and $\text{Im}[R_v^{\text{eq}}(\omega)] = \frac{N\lambda\omega}{(N+1)^2\lambda^2 + \omega^2}$.

In a similar manner, the departure from equilibrium can be expressed in terms of the displacement power-spectral density, as in Eq.(22). This allows the deviation from equilibrium to be quantified as

$$\mathcal{I}_x(\omega) = \tilde{C}_x(\omega) - \tilde{C}_x^{\text{eq}}(\omega) \quad (25)$$

where the power-spectral density $\tilde{C}_x^{\text{eq}}(\omega)$ in the equilibrium limit, i.e., $\tau_b, \tau_s \rightarrow 0$ and $\mathcal{D}_b = \mathcal{D}_s = D_{\text{eq}}$, as

$$\tilde{C}_x^{\text{eq}}(\omega) = 2D_{\text{eq}} \left[1 + \frac{N^2\lambda^2}{\lambda^2 + \omega^2} \right] \frac{\lambda^2 + \omega^2}{\omega^2[\lambda^2(1+N)^2 + \omega^2]} = \frac{2D_{\text{eq}}}{\omega^2} \frac{\lambda^2(1+N^2) + \omega^2}{\lambda^2(1+N)^2 + \omega^2} \quad (26)$$

The departures from equilibrium with changing reciprocity parameter are illustrated in Fig. 1. We plot the expressions in Eqs. (23) and (25) using $v_s = v_b = 1.0$ and $D_s^{\text{rot}} = D_b^{\text{rot}} = 10.0$, corresponding to $\tau_s = \tau_b = 0.1$ and $\mathcal{D}_s = \mathcal{D}_b = 0.1$. The equilibrium limit is recovered by setting $\lambda = \Lambda$ and $\tau_s, \tau_b \rightarrow 0$; thus, small persistence times and equal diffusivities provide a reference for quantifying departures from equilibrium when $\lambda \neq \Lambda$, i.e., $\chi \neq 1$.

Figures (a) and (b) show $\mathcal{I}_v(\omega)$ and $\mathcal{I}_x(\omega)$, respectively, as functions of the non-reciprocal parameter χ for different modes ω . For $N = 1$, strong divergence occurs for low- ω modes near $\chi = -1$ ($\lambda = -\Lambda$), while at large ω deviations remain small and no divergence is observed. As expected, deviations vanish in the reciprocal limit ($\lambda = \Lambda$, $\chi = 1$).

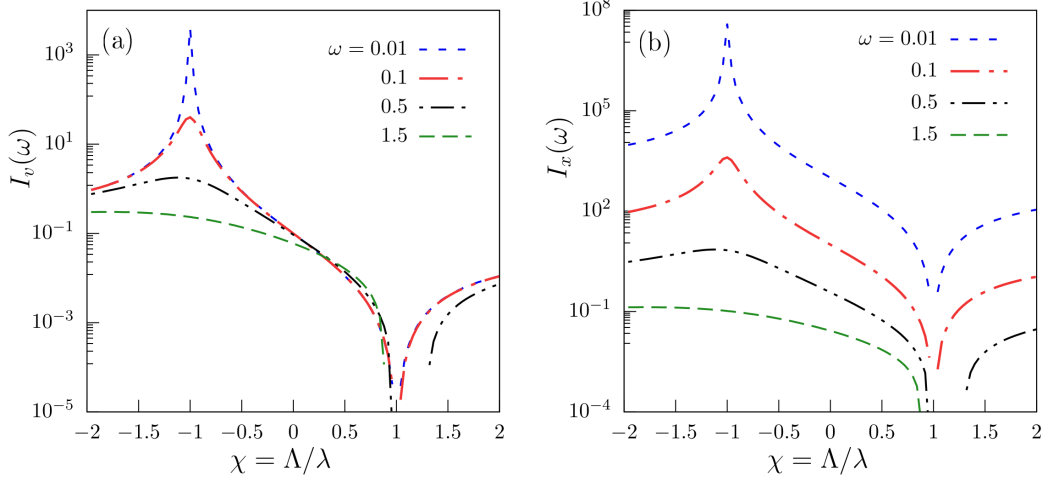


FIG. 1. Plots of the nonequilibrium departures $I_v(\omega)$ in (a) and $I_x(\omega)$ in (b) as functions of the nonreciprocal parameter $\chi = \Lambda/\lambda$ for different values of ω . The results are obtained using Eqs. (23) and (25), respectively. The remaining parameters for both plots are set to $\mathcal{D}_s = \mathcal{D}_b = 0.1$ with $\tau_s = \tau_b = 0.1$ and $D_{\text{eq}} = 0.1$.

E. Mean-squared displacement

The Fourier transform of Eq. (6) provides

$$i\omega \tilde{X}_s(\omega) + i\omega N\Lambda \tilde{X}_s(\omega) \tilde{\mathcal{G}}(\omega) = \tilde{\eta}_s^{\text{eff}}(\omega) = \tilde{\zeta}(\omega) + N\Lambda \tilde{\xi}(\omega) \tilde{\mathcal{G}}(\omega) \quad (27)$$

where $\tilde{X}_s(\omega) = \int_{-\infty}^{\infty} X_s(t) e^{-i\omega t} dt$, $\tilde{\zeta}(\omega) = \int_{-\infty}^{\infty} \zeta(t) e^{-i\omega t} dt$ and $\tilde{\zeta}_b(\omega) = N\Lambda \tilde{\xi}(\omega) \tilde{\mathcal{G}}(\omega)$ can be obtained using the convolution form (shown in Appendix B) where $\tilde{\xi}(\omega) = \int_{-\infty}^{\infty} \xi(t) e^{-i\omega t} dt$. Thus we finally get

$$\tilde{X}_s(\omega) = \frac{\tilde{\zeta}(\omega) + \tilde{\zeta}_b(\omega)}{i\omega \left[1 + N\Lambda \tilde{\mathcal{G}}(\omega) \right]} \quad (28)$$

where $\tilde{\mathcal{G}}(\omega)$ is given in Eq. (14). The MSD can now explicitly be written using Eq. (28) as,

$$\Delta_s(t) = \langle [X_s(t) - X_s(0)]^2 \rangle = \frac{1}{4\pi^2} \int_{-\infty}^{\infty} \int_{-\infty}^{\infty} \frac{\langle \tilde{\eta}_s^{\text{eff}}(\omega_1) \tilde{\eta}_s^{\text{eff}}(\omega_2) \rangle (e^{i\omega_1 t} - 1)(e^{i\omega_2 t} - 1)}{(i\omega_1)(i\omega_2) \left[1 + N\Lambda \tilde{\mathcal{G}}(\omega_1) \right] \left[1 + N\Lambda \tilde{\mathcal{G}}(\omega_2) \right]} d\omega_1 d\omega_2, \quad (29)$$

where, we used the inverse Fourier transform $X_s(t) = \frac{1}{2\pi} \int_{-\infty}^{\infty} \tilde{X}_s(\omega) e^{i\omega t} d\omega$.

Separating the effective noise correlation into two parts, and using Eqs. (8) and (9), the MSD takes the form

$$\Delta_s(t) = \frac{1}{4\pi^2} \left[\mathcal{I}_s(t) + \mathcal{I}_b(t) \right], \quad (30)$$

where $\mathcal{I}_s(t)$ and $\mathcal{I}_b(t)$ corresponds to the contributions from the tracer itself and the influence of the bath, respectively. The calculations to find out the explicit forms for $\mathcal{I}_s(t)$ and $\mathcal{I}_b(t)$ using $\langle \tilde{\eta}_s^{\text{eff}}(\omega_1) \tilde{\eta}_s^{\text{eff}}(\omega_2) \rangle = \langle \tilde{\zeta}_b(\omega_1) \tilde{\zeta}_b(\omega_2) \rangle + \langle \tilde{\zeta}(\omega_1) \tilde{\zeta}(\omega_2) \rangle$ are shown in Appendix D. Their final expressions are:

$$\mathcal{I}_s(t) = \frac{8\pi^2 \mathcal{D}_s}{[1 - c^2 \tau_s^2]} \left[\frac{\lambda^2}{c^3} (ct - 1 + e^{-ct}) - \lambda^2 \tau_s^3 \left(\frac{t}{\tau_s} - 1 + e^{-t/\tau_s} \right) - \frac{1}{c} (e^{-ct} - 1) + \tau_s (e^{-t/\tau_s} - 1) \right] \quad (31)$$

and

$$\mathcal{I}_b(t) = \frac{8\pi^2 \mathcal{D}_b N^2 \Lambda^2}{(1 - \tau_b^2 c^2)} \left[\frac{1}{c^3} (ct - 1 + e^{-ct}) - \tau_b^3 \left(\frac{t}{\tau_b} - 1 + e^{-t/\tau_b} \right) \right], \quad (32)$$

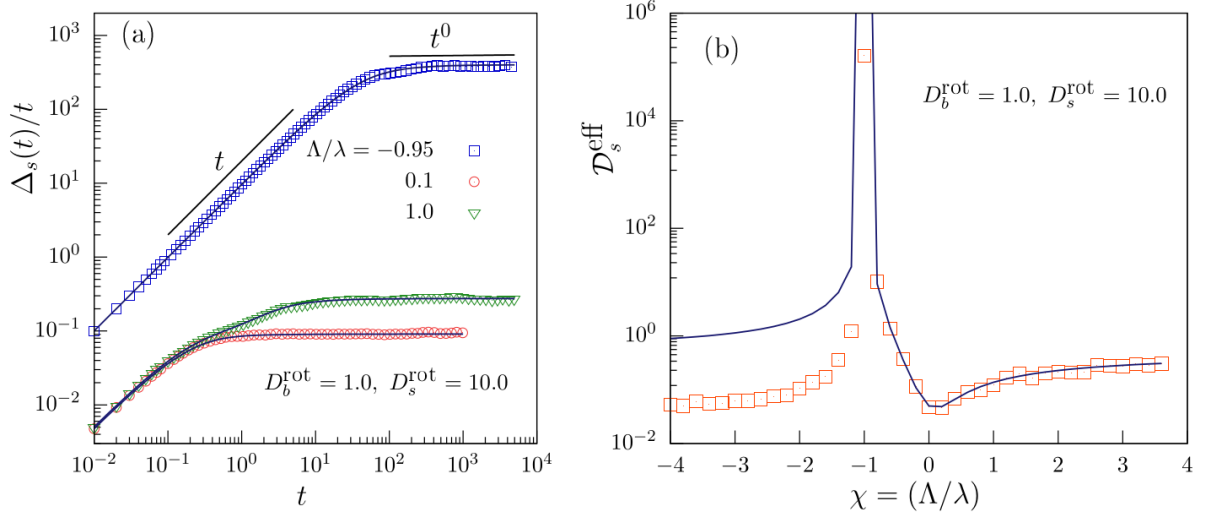


FIG. 2. (a) Mean-squared displacement (MSD) scaled by time, $\Delta_s(t)/t$, as a function of t for a tracer attached to a bath particle, for different values of the non-reciprocal parameter $\chi = \Lambda/\lambda$. Solid lines indicate the analytical prediction from Eq. (30). Enhanced diffusivity is observed for $\Lambda/\lambda = -0.95$. Reference lines indicate the ballistic ($\propto t$) and diffusive ($\propto t^0$) regimes. (b) Effective diffusivity D_s^{eff} of the tracer as a function of χ . Giant diffusivity emerges near $\chi = -1$, with the solid line showing the theoretical form from Eq. (34). Data points correspond to results from ABP simulations.

where, $c = (\lambda + N\Lambda)$ is an effective coupling strength. This exact closed-form expression for the MSD can be analyzed at various time regimes. The generic term $(t/\tau - 1 + e^{-t/\tau})$, which appears in several contributions in Eqs. (31) and (32), gives rise to ballistic-to-diffusive crossovers at the corresponding characteristic times τ . In the following, we examine the behavior of the full MSD in the short- and long-time limits.

In the short time limit the full MSD exhibits ballistic scaling

$$\Delta_s(t)|_{t \rightarrow 0} = \left[\frac{\mathcal{D}_s}{(1 + c\tau_s)} \left(\frac{\lambda^2}{c} + \frac{1}{\tau_s} \right) + \frac{\mathcal{D}_b \Lambda^2}{c(1 + c\tau_b)} \right] t^2. \quad (33)$$

In the long time limit it displays a diffusive behavior

$$\Delta_s(t)|_{t \rightarrow \infty} = 2 \left[\frac{\mathcal{D}_s}{\left(1 + N\Lambda/\lambda\right)^2} + \frac{\mathcal{D}_b (N\Lambda/\lambda)^2}{\left(1 + N\Lambda/\lambda\right)^2} \right] t \equiv 2\mathcal{D}_s^{\text{eff}} t. \quad (34)$$

Recall that $\mathcal{D}_s = v_s^2 \tau_s$ and $\mathcal{D}_b = v_b^2 \tau_b$ stand for the effective diffusivities of the tracer and bath particles, respectively. Note that the dynamics here depend upon the activity as well as the generic non-reciprocal system-bath coupling which may lead to qualitatively profound effect, particularly, when the ratio between the coupling strengths $\chi = \Lambda/\lambda$ approaches $-1/N$. Note that the diffusivity calculated from MSD in Eq. (34) agrees with D_{eff} obtained from $\tilde{C}_v(\omega = 0)$ in Eq. (21). Clearly, in the large- N limit the effective diffusivity is governed by the bath particles. For positive χ , D_{eff} increases monotonically with N and saturates at \mathcal{D}_b . In contrast, for negative χ it exhibits a nonmonotonic dependence on N , diverging as $N \approx -1/\chi$ before eventually approaching its asymptotic saturation value.

F. Numerical Verifications

We validate our analytical results through numerical simulations in which a tracer is coupled to a bath particle, with both modeled as active Brownian particles (ABPs). The simulations are based on Eq. (1), with $\xi_i = v_b \cos \theta_i^b$ where the bath particle orientation evolves as $\dot{\theta}_i^b = \sqrt{2D_b^{\text{rot}}} \eta_i^b(t)$. Similarly, for the tracer, $\zeta = v_s \cos \theta_s$ with $\dot{\theta}_s = \sqrt{2D_s^{\text{rot}}} \eta_s(t)$, where $\eta_s(t)$ and $\eta_i^b(t)$ are independent Gaussian white noises with unit variance.

Equations (1) are integrated using the Euler-Maruyama scheme with a time step $\delta t = 0.01$. For $\chi < 0$, the tracer follows the bath particle while the bath particle moves away from the tracer, and vice versa. To ensure local, non-divergent repulsion in the harmonic non-reciprocal interaction, a finite cutoff distance $x_c = 5.0$ is applied. Simulation results with explicit parameter values are shown in Fig. 2.

In Fig. 2, the active velocities of both the tracer and bath particles are set to $v_s = v_b = 1.0$. The corresponding rotational diffusion coefficients are $D_s^{\text{rot}} = 10.0$ for the tracer and $D_b^{\text{rot}} = 1.0$ for the bath, yielding persistence times $\tau_s = 0.1$ and $\tau_b = 1.0$, respectively. Consequently, the bath particle exhibits stronger activity. The effective diffusivities are $\mathcal{D}_s = 0.05$ for the tracer and $\mathcal{D}_b = 0.5$ for the bath.

Figure 2(a) shows the tracer mean-square displacement (MSD) for three values of the non-reciprocity parameter $\chi = 0.1, 1.0$, and -0.95 . The case $\chi = 1.0$ corresponds to reciprocal interactions, whereas $\chi = -0.95$ realizes run-and-chase dynamics, leading to a markedly enhanced diffusivity. The solid lines represent Eq. (30) and are in exact agreement with the simulation data.

Figure 2(b) displays the effective tracer diffusivity $\mathcal{D}_s^{\text{eff}}$ as a function of χ , showing excellent agreement with the analytical prediction in Eq. (34) for $\chi > -1$. In particular, the theory accurately captures the divergence as $\chi \rightarrow -1$. This divergence corresponds to the maximal departure of the coupled tracer-bath system from equilibrium, as illustrated in Fig. 1.

For $\chi < -1$, however, the finite interaction cutoff x_c becomes crucial in producing physically reasonable dynamics in the simulations. The harmonic approximation employed in the analytical treatment effectively assumes increasingly strong repulsion at large separations, which is unphysical. As a result, while the theory correctly predicts the qualitative trend of decreasing effective diffusivity away from resonance, it fails to quantitatively reproduce the numerical results in the presence of a finite interaction cutoff.

IV. CONCLUSIONS

In this work, we have developed a minimal yet analytically tractable framework to investigate tracer dynamics in active systems with non-reciprocal interactions. By considering a tracer harmonically coupled to a bath of particles and systematically integrating out the bath degrees of freedom, we derived an overdamped generalized Langevin equation featuring a non-Markovian memory kernel and colored noise. We showed that this colored noise has two distinct physical origins, arising both from the intrinsic persistence of active particles and from the tracer-bath interactions themselves. Our formulation is fully general, applying to both active and passive tracers and baths, with the passive limit recovered smoothly by taking the persistence time to zero at fixed single-particle diffusivity. Finally, we demonstrated that equilibrium is restored only for reciprocal interactions, clearly identifying non-reciprocity as a fundamental source of nonequilibrium behavior.

Within this unified framework, we obtained exact analytical expressions for key dynamical observables of the tracer, obtaining the velocity and position response functions, the mean-squared displacement, and the asymptotic effective diffusivity. Furthermore, by deriving a generalized fluctuation-dissipation relation around the nonequilibrium steady state, we quantified departures from equilibrium in a systematic manner. The development of this formalism and the exact characterization of tracer dynamics constitute the first main contribution of this work.

Our analysis reveals that increasing activity enhances nonequilibrium departures, as expected. Strikingly, we find that for sufficiently strong negative non-reciprocity – at values that depend on the number of bath particles – the low-frequency departures from equilibrium exhibit pronounced divergences. These divergences directly influence the long-time tracer diffusivity, giving rise to a regime of unusually large diffusivity that we termed as *giant diffusivity*. We confirmed this prediction through numerical simulations of active Brownian particles, demonstrating the robustness of the effect beyond the idealized analytical model. The identification and characterization of this non-reciprocity-induced giant diffusivity represent the second main contribution of our study.

More broadly, our results highlight the significant role of non-reciprocal interactions in shaping transport in active systems. Giant diffusivity emerges as a generic outcome of non-reciprocal interactions, enabling enhanced spatial exploration. These phenomena should be accessible in experiments on both synthetic and biological active matter, including predator-prey systems. Overall, our work points to non-reciprocity as a promising design principle for tuning transport and exploration in nonequilibrium systems.

Acknowledgment: We thank Abhishek Dhar for discussions. D.C. acknowledges research grants from DAE, India (1603/2/2020/IoP/R&D-II/150288), and thanks ICTS, Bangalore for an Associateship and support during the meeting “Active Matter and Beyond” (code: ICTS/AMAB2024/11). S.P. acknowledges the University of Delhi for providing financial assistance through the Faculty Research Programme under Grant-IOE (Ref. No. IOE/2024-25/12/FRP).

Appendix A: Tracer dynamics

$$\frac{dX_s}{dt} + N\Lambda X_s = \xi_s + \Lambda e^{-\lambda t} \sum_{i=1}^N x_i(0) + \Lambda \sum_{i=1}^N \left(\int_0^t \xi_i(t') e^{-\lambda(t-t')} dt' + \lambda \int_0^t X_s(t') e^{-\lambda(t-t')} dt' \right), \quad (\text{A1})$$

where the summation over N describes contribution from all independent bath particles.

The contribution from the second term vanishes either by choosing the initial conditions of the bath such that $\sum_i x_i(0) = 0$, or equivalently by considering large times t where the system has reached the steady state. Since the contributions from individual bath particles are independent, the equation for X_s reduces to

$$\frac{dX_s}{dt} + N\Lambda X_s = \xi_s + N\Lambda \int_0^t \xi(t') e^{-\lambda(t-t')} dt' + N\Lambda \lambda \int_0^t X_s(t') e^{-\lambda(t-t')} dt'. \quad (\text{A2})$$

Appendix B: Fourier transform of the convolution form

The convolution form

$$f(\omega) = Nk\lambda \int_{-\infty}^{\infty} \left[\int_{-\infty}^{\infty} X_s(t') e^{-\lambda(t-t')} dt' \right] e^{-i\omega t} dt, \quad (\text{B1})$$

can be rewritten, interchanging the integrals as

$$f(\omega) = Nk\lambda \int_{-\infty}^{\infty} X_s(t') \left[\int_{-\infty}^{\infty} e^{-\lambda s} e^{-i\omega s} ds \right] e^{-i\omega t'} dt'$$

where $s = t - t'$. As a result, it can be simplified in the product form

$$f(\omega) = Nk\lambda \tilde{C}(\omega) \tilde{X}_s(\omega) \quad (\text{B2})$$

Appendix C: Noise correlation in Fourier space

Here we calculate the explicit forms of the correlations $\langle \tilde{\zeta}_b(\omega_1) \tilde{\zeta}_b(\omega_2) \rangle$ and $\langle \tilde{\zeta}(\omega_1) \tilde{\zeta}(\omega_2) \rangle$.

As $\zeta_b(t)$ is related to the noise $\xi(t)$ as $\zeta_b(t) = N\Lambda \int_{-\infty}^t \xi(t') \mathcal{G}(t-t') dt'$, thus the Fourier transform gives

$$\tilde{\zeta}_b(\omega) = N\Lambda \tilde{\xi}(\omega) \tilde{\mathcal{G}}(\omega)$$

We use the two-time correlation function of the active noise associated with the bath particles (Eq. (3))

$$\langle \xi_i(t_1) \xi_j(t_2) \rangle = v_b^2 \delta_{ij} e^{-|t_1 - t_2|/\tau_b}$$

Using this expression, we compute the correlation function in Fourier space:

$$\langle \tilde{\xi}(\omega_1) \tilde{\xi}(\omega_2) \rangle = \int_{-\infty}^{\infty} \int_{-\infty}^{\infty} \langle \xi(t_1) \xi(t_2) \rangle e^{-i\omega_1 t_1} e^{-i\omega_2 t_2} dt_1 dt_2 = v_b^2 (I_1 + I_2) \quad (\text{C1})$$

where I_1 corresponds to the time ordering $t_1 > t_2$, and I_2 to $t_2 > t_1$. We first evaluate I_1 :

$$I_1 = \int_{-\infty}^{\infty} dt_1 \int_{-\infty}^{t_1} dt_2 e^{-(t_1 - t_2)/\tau_b} e^{-i\omega_1 t_1} e^{-i\omega_2 t_2} dt_1 dt_2 = \frac{2\pi}{(1/\tau_b - i\omega_2)} \delta(\omega_1 + \omega_2).$$

By symmetry, the contribution from the opposite time ordering ($t_2 > t_1$) is

$$I_2 = \frac{2\pi}{(1/\tau_b - i\omega_1)} \delta(\omega_1 + \omega_2).$$

Combining I_1 and I_2 we obtain

$$\langle \tilde{\xi}(\omega_1)\tilde{\xi}(\omega_2) \rangle = 2\pi v_b^2 \left[\frac{1}{1/\tau_b - i\omega_1} + \frac{1}{1/\tau_b - i\omega_2} \right] \delta(\omega_1 + \omega_2) \quad (\text{C2})$$

This result yields the noise correlation in ω -space as

$$\langle \tilde{\zeta}_b(\omega_1)\tilde{\zeta}_b(\omega_2) \rangle = N^2 \Lambda^2 \langle \tilde{\xi}(\omega_1)\tilde{\xi}(\omega_2) \rangle \tilde{\mathcal{G}}(\omega_1)\tilde{\mathcal{G}}(\omega_2) \quad (\text{C3})$$

$$= 2\pi N^2 \Lambda^2 v_b^2 \left[\frac{1}{1/\tau_b - i\omega_1} + \frac{1}{1/\tau_b - i\omega_2} \right] \frac{\delta(\omega_1 + \omega_2)}{(\lambda + i\omega_1)(\lambda + i\omega_2)} \quad (\text{C4})$$

where we have used $\tilde{\mathcal{G}}(\omega) = \frac{1}{\lambda + i\omega}$.

Thus, the the final expression for the bath-induced noise correlation in Fourier space is

$$\langle \tilde{\zeta}_b(\omega_1)\tilde{\zeta}_b(\omega_2) \rangle = 2\pi N^2 \Lambda^2 v_b^2 \left[\frac{1}{1/\tau_b - i\omega_1} + \frac{1}{1/\tau_b - i\omega_2} \right] \frac{\delta(\omega_1 + \omega_2)}{(\lambda + i\omega_1)(\lambda + i\omega_2)} \equiv \mathcal{B}_1(\omega) \delta(\omega_1 + \omega_2) \quad (\text{C5})$$

The amplitude of the correlation $\mathcal{B}_1(\omega)$ can be obtained by setting $\omega_1 = -\omega_2 = \omega$,

$$\mathcal{B}_1(\omega) = \frac{N^2 \Lambda^2}{\lambda^2 + \omega^2} \frac{4\pi v_b^2 \tau_b}{1 + \omega^2 \tau_b^2} = \frac{N^2 \Lambda^2}{\lambda^2 + \omega^2} \frac{4\pi \mathcal{D}_b}{1 + \omega^2 \tau_b^2} \quad (\text{C6})$$

In the equilibrium limit $\tau_b \rightarrow 0$, with $\lambda = \Lambda$ and $\mathcal{D}_b = D_{\text{eq}}$, this expression reduces to

$$\mathcal{B}_1^{\text{eq}}(\omega) = 4\pi D_{\text{eq}} \frac{N^2 \lambda^2}{\lambda^2 + \omega^2}$$

Similarly, for $\mathcal{I}_s(t)$, we express the correlation function of the noise $\tilde{\zeta}(\omega)$ as

$$\langle \tilde{\zeta}(\omega_1)\tilde{\zeta}(\omega_2) \rangle = 2\pi \mathcal{D}_s \left[\frac{1}{1 - i\omega_1 \tau_s} + \frac{1}{1 - i\omega_2 \tau_s} \right] \delta(\omega_1 + \omega_2) \equiv \mathcal{B}_2(\omega) \delta(\omega_1 + \omega_2). \quad (\text{C7})$$

As before, the amplitude of the correlation $\mathcal{B}_2(\omega)$ is given by

$$\mathcal{B}_2(\omega) = \frac{4\pi \mathcal{D}_s}{1 + \omega^2 \tau_s^2}. \quad (\text{C8})$$

In the equilibrium limit $\tau_s \rightarrow 0$, and $\mathcal{D}_s = D_{\text{eq}}$, this expression reduces to

$$\mathcal{B}_2^{\text{eq}}(\omega) = 4\pi D_{\text{eq}}.$$

The forms for $\mathcal{B}_1(\omega)$ and $\mathcal{B}_2(\omega)$ are used in Eq. (20).

Appendix D: Explicit forms for $\mathcal{I}_s(t)$ and $\mathcal{I}_b(t)$

Here we calculate the explicit expressions of $\mathcal{I}_s(t)$ and $\mathcal{I}_b(t)$ as mentioned in Eq. (30). The expressions for $\mathcal{I}_s(t)$ and $\mathcal{I}_b(t)$ are following:

$$\mathcal{I}_s(t) = \int_{-\infty}^{\infty} \int_{-\infty}^{\infty} \frac{\langle \tilde{\zeta}(\omega_1)\tilde{\zeta}(\omega_2) \rangle (e^{i\omega_1 t} - 1)(e^{i\omega_2 t} - 1)}{(i\omega_1)(i\omega_2) \left[1 + N\Lambda \tilde{\mathcal{G}}(\omega_1) \right] \left[1 + N\Lambda \tilde{\mathcal{G}}(\omega_2) \right]} d\omega_1 d\omega_2 \quad (\text{D1})$$

and

$$\begin{aligned} \mathcal{I}_b(t) &= \int_{-\infty}^{\infty} \int_{-\infty}^{\infty} \frac{\langle \tilde{\zeta}_b(\omega_1)\tilde{\zeta}_b(\omega_2) \rangle (e^{i\omega_1 t} - 1)(e^{i\omega_2 t} - 1)}{(i\omega_1)(i\omega_2) \left[1 + N\Lambda \tilde{\mathcal{G}}(\omega_1) \right] \left[1 + N\Lambda \tilde{\mathcal{G}}(\omega_2) \right]} d\omega_1 d\omega_2 \\ &= N^2 \Lambda^2 \int_{-\infty}^{\infty} \int_{-\infty}^{\infty} \frac{\langle \tilde{\xi}(\omega_1)\tilde{\xi}(\omega_2) \rangle \tilde{\mathcal{G}}(\omega_1)\tilde{\mathcal{G}}(\omega_2) (e^{i\omega_1 t} - 1)(e^{i\omega_2 t} - 1)}{(i\omega_1)(i\omega_2) \left[1 + N\Lambda \tilde{\mathcal{G}}(\omega_1) \right] \left[1 + N\Lambda \tilde{\mathcal{G}}(\omega_2) \right]} d\omega_1 d\omega_2. \end{aligned} \quad (\text{D2})$$

We first compute the numerator of $\mathcal{I}_b(t)$. The denominator is the same for both the terms. Its explicit calculation shows

$$\left[1 + N\Lambda\tilde{\mathcal{G}}(\omega_1)\right]\left[1 + N\Lambda\tilde{\mathcal{G}}(\omega_2)\right] = 1 + N\Lambda\left(\frac{1}{\lambda + i\omega_1} + \frac{1}{\lambda + i\omega_2}\right) + \frac{N^2\Lambda^2}{(\lambda + i\omega_1)(\lambda + i\omega_2)}. \quad (\text{D3})$$

In the above calculation, we used $\tilde{\mathcal{G}}(\omega) = \frac{1}{\lambda + i\omega}$.

Using Eqs. (C5) and (C7), we obtain relatively compact expressions for the integrals $\mathcal{I}_s(t)$ and $\mathcal{I}_b(t)$:

$$\mathcal{I}_s(t) = 4\pi\mathcal{D}_s \int_{-\infty}^{\infty} \frac{2[1 - \cos(\omega t)]}{\omega^2(1 + \omega^2\tau_s^2)} \frac{(\lambda^2 + \omega^2) d\omega}{[(\lambda^2 + \omega^2) + 2\lambda\Lambda N + \Lambda^2 N^2]} \quad (\text{D4})$$

and

$$\mathcal{I}_b(t) = 4\pi\mathcal{D}_b \int_{-\infty}^{\infty} \frac{2[1 - \cos(\omega t)]}{\omega^2(1 + \omega^2\tau_b^2)} \frac{N^2\Lambda^2 d\omega}{[(\lambda^2 + \omega^2) + 2\lambda\Lambda N + \Lambda^2 N^2]} \quad (\text{D5})$$

The results of these integrations are presented in Eqs. (31) and (32) of the main text.

[1] W. B. Russel, Brownian motion of small particles suspended in liquids, *Annual Review of Fluid Mechanics* **13**, 425–455 (1981).

[2] R. N. Zia, Active and passive microrheology: Theory and simulation, *Annual Review of Fluid Mechanics* **50**, 371 (2018).

[3] X. L. Wu and A. Libchaber, Particle diffusion in a quasi-two-dimensional bacterial bath, *Phys. Rev. Lett.* **84**, 3017 (2000).

[4] K. Kanazawa, T. G. Sano, A. Cairol, and A. Baule, Loopy lévy flights enhance tracer diffusion in active suspensions, *Nature* **579**, 364–367 (2020).

[5] A. Baule, Universal poisson statistics of a passive tracer diffusing in dilute active suspensions, *Proceedings of the National Academy of Sciences* **120**, e2308226120 (2023).

[6] B. Wang, S. M. Anthony, S. C. Bae, and S. Granick, Anomalous yet Brownian, *PNAS* **106**, 15160–15164 (2009).

[7] I. M. Tolic-Norrelykke, E. L. Munteanu, G. Thon, L. Oddershede, and K. Berg-Sorensen, Anomalous diffusion in living yeast cells, *Phys. Rev. Lett.* **93**, 078102 (2004).

[8] C. Lutz, M. Kollmann, and C. Bechinger, Single-file diffusion of colloids in one-dimensional channels, *Phys. Rev. Lett.* **93**, 026001 (2004).

[9] P. Dieterich, R. Klages, R. Preuss, and A. Schwab, Anomalous dynamics of cell migration, *PNAS* **105**, 459–463 (2008).

[10] R. Golestanian, Anomalous diffusion of symmetric and asymmetric active colloids, *Phys. Rev. Lett.* **102**, 188305 (2009).

[11] N. Gupta, A. Chaudhuri, and D. Chaudhuri, Morphological and dynamical properties of semiflexible filaments driven by molecular motors, *Phys. Rev. E* **99**, 1–10 (2019).

[12] A. Shee, A. Dhar, and D. Chaudhuri, Active Brownian particles: mapping to equilibrium polymers and exact computation of moments, *Soft Matter* **16**, 4776–4787 (2020).

[13] M. Patel and D. Chaudhuri, Exact moments and re-entrant transitions in the inertial dynamics of active Brownian particles, *New J. Phys.* **25**, 123048 (2023).

[14] S. Paul, A. Dhar, and D. Chaudhuri, Dynamical crossovers and correlations in a harmonic chain of active particles, *Soft Matter* **1**, (2024).

[15] M. Patel, S. Paul, and D. Chaudhuri, Crossover dynamics and non-gaussian fluctuations in inertial active chains [10.48550/arXiv.2511.13270](https://arxiv.org/abs/2511.13270) (2025), arXiv:2511.13270 [cond-mat].

[16] O. Bénichou, P. Illien, G. Oshanin, A. Sarracino, and R. Voituriez, Tracer diffusion in crowded narrow channels: Topical review, *Journal of Physics: Condensed Matter* **30**, 443001 (2018).

[17] T. E. Harris, Diffusion with “collisions” between particles, *Journal of Applied Probability* **2**, 323 (1965).

[18] D. G. Levitt, Dynamics of a single-file pore: Non-fickian behavior, *Physical Review A* **8**, 3050 (1973).

[19] P. M. Chaikin and T. C. Lubensky, *Principles of Condensed Matter Physics* (Cambridge University Press, Cambridge, 2012).

[20] E. W. Burkholder and J. F. Brady, Tracer diffusion in active suspensions, *Physical Review E* **95**, 052605 (2017).

[21] E. W. Burkholder and J. F. Brady, Nonlinear microrheology of active Brownian suspensions, *Soft Matter* **16**, 1034 (2020).

[22] O. Granek, Y. Kafri, and J. Tailleur, Anomalous transport of tracers in active baths, *Phys. Rev. Lett.* **129**, 038001 (2022).

[23] E. Barkai, Y. Garini, and R. Metzler, Strange kinetics of single molecules in living cells, *Physics today* **65**, 29 (2012).

[24] F. Höfling and T. Franosch, Anomalous transport in the crowded world of biological cells, *Rep. Prog. Phys.* **76**, 046602 (2013).

[25] É. Fodor, M. Guo, N. Gov, P. Visco, D. Weitz, and F. Van Wijland, Activity-driven fluctuations in living cells, *Europhys. Lett.* **110**, 48005 (2015).

[26] M. Otten, A. Nandi, D. Arcizet, M. Gorelashvili, B. Lindner, and D. Heinrich, Local motion analysis reveals impact of the dynamic cytoskeleton on intracellular subdiffusion, *Biophys. J.* **102**, 758 (2012).

[27] T. S. V. Podestá, T. V. Rosembach, A. A. Dos Santos, and M. L. Martins, Anomalous diffusion and q-weibull velocity distributions in epithelial cell migration, *PLoS ONE* **12**, 1–19 (2017).

[28] T. Harada and S.-i. Sasa, Equality connecting energy dissipation with a violation of the fluctuation-response relation, *Phys. Rev. Lett.* **95**, 130602 (2005).

[29] A. Dechant and S. I. Sasa, Fluctuation-response inequality out of equilibrium, *PNAS* **117**, 6430–6436 (2020).

[30] S. Dal Cengio, D. Levis, and I. Pagonabarraga, Linear response theory and green-kubo relations for active matter, *Physical Review Letters* **123**, 238003 (2019).

[31] S. D. Cengio, D. Levis, and I. Pagonabarraga, Fluctuation–dissipation relations in the absence of detailed balance: formalism and applications to active matter, *J. Stat. Mech.: Th. Expt.* **2021**, 043201 (2021).

[32] T. Speck and U. Seifert, Restoring a fluctuation-dissipation theorem in a nonequilibrium steady state, *Europhys. Lett.* **74**, 391 (2006).

[33] J. Prost, J.-F. Joanny, and J. M. R. Parrondo, Generalized fluctuation-dissipation theorem for steady-state systems, *Phys. Rev. Lett.* **103**, 090601 (2009).

[34] D. Chaudhuri, Active brownian particles: Entropy production and fluctuation response, *Physical Review E* **90**, 022131 (2014).

[35] D. Chaudhuri and A. Chaudhuri, Modified fluctuation-dissipation and Einstein relation at nonequilibrium steady states, *Phys. Rev. E* **85**, 021102 (2012), 1201.4525.

[36] D. Loi, S. Mossa, and L. F. Cugliandolo, Effective temperature of active complex matter, *Soft Matter* **7**, 3726 (2011), 1012.2745.

[37] L. F. Cugliandolo, G. Gonnella, and I. Petrelli, Effective Temperature in Active Brownian Particles, *Fluct. Noise Lett.* **18**, 1940008 (2019).

[38] S. Mandal, B. Liebchen, and H. Löwen, Motility-Induced Temperature Difference in Coexisting Phases, *Phys. Rev. Lett.* **123**, 228001 (2019), 1902.06116.

[39] I. Petrelli, L. F. Cugliandolo, G. Gonnella, and A. Suma, Effective temperatures in inhomogeneous passive and active bidimensional Brownian particle systems, *Phys. Rev. E* **102**, 012609 (2020), 2005.02303.

[40] L. Caprini and U. M. B. Marconi, Active matter at high density: Velocity distribution and kinetic temperature, *J. Chem. Phys.* **153**, 184901 (2020), 2009.07234.

[41] H. Mori, Transport, collective motion, and brownian motion, *Progress of Theoretical Physics* **33**, 423–455 (1965).

[42] R. Zwanzig, *Nonequilibrium statistical mechanics* (Oxford university press, 2001).

[43] S. S. Khali, F. Peruani, and D. Chaudhuri, When an active bath behaves as an equilibrium one, *Physical Review E* **109**, 024120 (2024).

[44] R. Golestanian, Non-reciprocal active-matter: a tale of “loving hate, brawling love” across the scales, *Europhys. News* **55**, 12 (2024).

[45] A. Dinelli, J. O’Byrne, A. Curatolo, Y. Zhao, P. Sollich, and J. Tailleur, Non-reciprocity across scales in active mixtures, *Nat. Comm.* **14**, 7035 (2023).

[46] Z. You, A. Baskaran, and M. C. Marchetti, Nonreciprocity as a generic route to traveling states, *PNAS* **117**, 19767–19772 (2020).

[47] M. Fruchart, R. Hanai, P. B. Littlewood, and V. Vitelli, Non-reciprocal phase transitions, *Nature* **592**, 363–369 (2021).

[48] S. Saha, J. Agudo-Canalejo, and R. Golestanian, Scalar active mixtures: The nonreciprocal cahn-hilliard model, *Physical Review X* **10**, 041009 (2020).

[49] S. A. M. Loos, S. H. L. Klapp, and T. Martynec, Long-range order and directional defect propagation in the nonreciprocal xy model with vision cone interactions, *Phys. Rev. Lett.* **130**, 198301 (2023).

[50] S. A. M. Loos and S. H. L. Klapp, Irreversibility, heat and information flows induced by non-reciprocal interactions, *New Journal of Physics* **22**, 123051 (2020).

[51] R. K. Gupta, R. Kant, H. Soni, A. K. Sood, and S. Ramaswamy, Active nonreciprocal attraction between motile particles in an elastic medium, *Phys. Rev. E* **105**, 064602 (2022), arXiv: 2007.04860 publisher: American Physical Society.

[52] Z. Zhang and R. Garcia-Millan, Entropy production of nonreciprocal interactions, *Phys. Rev. Res.* **5**, L022033 (2023).

[53] R. Soto and R. Golestanian, Self-assembly of catalytically active colloidal molecules: Tailoring activity through surface chemistry, *Phys. Rev. Lett.* **112**, 068301 (2014).

[54] S. Saha, R. Golestanian, and S. Ramaswamy, Clusters, asters, and collective oscillations in chemotactic colloids, *Phys. Rev. E* **89**, 062316 (2014).

[55] H. Stark, Artificial chemotaxis of self-phoretic active colloids: Collective behavior, *Acc. Chem. Res.* **51**, 2681 (2018).

[56] B. Nasouri and R. Golestanian, Exact phoretic interaction of two chemically active particles, *Phys. Rev. Lett.* **124**, 168003 (2020).

[57] J. Grauer, H. Löwen, M. Be’er, and B. Liebchen, Swarm hunting and cluster ejections in chemically communicating active mixtures, *Sci. Rep.* **10**, 5594 (2020).

[58] N. S. Mandal, A. Sen, and R. D. Astumian, A molecular origin of non-reciprocal interactions between interacting active catalysts, *Chem* **10**, 1147–1159 (2024).

[59] F. A. Lavergne, H. Wendehenne, T. Bäuerle, and C. Bechinger, Group formation and cohesion of active particles with visual perception-dependent motility, *Science* **364**, 70 (2019).

[60] F. Schmidt, B. Liebchen, H. Löwen, and G. Volpe, Self-propel by spontaneous symmetry breaking, *Chem. Commun.* **54**, 11933 (2018).

- [61] L. Barberis and F. Peruani, Large-scale patterns in a minimal cognitive flocking model: Incidental leaders, nematic patterns, and aggregates, *Phys. Rev. Lett.* **117**, 248001 (2016).
- [62] R. S. Negi, R. G. Winkler, and G. Gompper, Emergent collective behavior of active Brownian particles with visual perception, *Soft Matter* **18**, 6167 (2022).
- [63] T. Bäuerle, A. Fischer, T. Speck, and C. Bechinger, Self-organization of active particles by quorum sensing rules, *Nat. Commun.* **9**, 3232 (2018).
- [64] A. Fischer, F. Schmid, and T. Speck, Quorum-sensing active particles with discontinuous motility, *Phys. Rev. E* **101**, 012601 (2020).
- [65] S. Nagano and Y. Maeda, Phase transitions in predator-prey systems, *Phys. Rev. E* **85**, 011915 (2012).
- [66] A. Sengupta, T. Kruppa, and H. Löwen, Chemotactic predator-prey dynamics, *Phys. Rev. E* **83**, 031914 (2011).
- [67] C. Xue and N. Goldenfeld, Stochastic predator-prey dynamics of transposons in the human genome, *Phys. Rev. Lett.* **117**, 208101 (2016).
- [68] P. J. Nahin, *Chases and Escapes: The Mathematics of Pursuit and Evasion* (Princeton University Press, Princeton, NJ, 2007).
- [69] R. Isaacs, *Differential Games: A Mathematical Theory with Applications to Warfare and Pursuit, Control and Optimization* (Wiley, New York, 1965).
- [70] J. G. Foreman, Differential search games with mobile hider, *SIAM Journal on Control and Optimization* **15**, 841 (1977).
- [71] G. Owen and G. H. McCormick, Finding a moving fugitive: A game-theoretic representation of search, *Computers and Operations Research* **35**, 1944 (2008).
- [72] Utilizing the equilibrium limit of $\tau_b, \tau_s \rightarrow 0$ and $\mathcal{D}_b = \mathcal{D}_s = D_{\text{eq}}$.